Numerical and modelling studies of the geogrid-reinforced ash-storage embankment in the conditions of the undermined territories

Rauan E. Lukpanov ✉ iD

Eurasian National University of L.N. Gumilyov, Department of Architecture and Civil Engineering,
2 Satpayev St, 010008, Astana, Kazakhstan

Abstract: The article presents the results of the study of the stability of the reinforced ash-storage embankment (ASE) of a functioning metallurgical plant. The purpose of the tests was to determine the numerical modelling correction factors based on the model test results. The model tests were performed at a scale of 1:30 to the full-scale embankment. The numerical modelling was a simulation of model testing in two tasks. The first task considered the simulation of model testing on a reduced scale (relative to ASE) of a real sheet, using the characteristics of an equivalent material. The second task considered the simulation of ash-and-slag mixtures on an *in situ* scale with real characteristics but under the conditions of the model tests. The quantitative assessment of each of the research methods, as well as the identified regularities of the stress–strain states of reinforced and unreinforced embankment, are presented in the article. Based on the results of the studies, a method of stability assessment by numerical modelling was obtained, the results of which reflect the most reliable condition of the stress-strain state of the reinforced embankment (since the results are subject to adjustment based on the regularities of the model, although still *in situ* tests).

Keywords: embankment, geogrid, geosynthetic, modelling, numerical analysis, reinforcement, slope, stability analysis

INTRODUCTION

The history of soil reinforcement dates back to ancient times. One of the most ancient and unique embodiments of mankind using the technique of soil reinforcement includes the ziggurat di Agar-Quif, located near Baghdad (Chang *et al.*, 2003). The modern use of geosynthetics to improve the properties of soils dates back to the mid-'60s of the 20th century in the United States (Berg and Collin, 1993). It was then that geosynthetic materials made of various polymers, usually having high tensile strength, were proposed (Shin and Young, 2006). The term "reinforced soil" was introduced by the French architect Henry Vidal, who developed Casagrande's concept. Casagrande was the first to point out that natural elements (reeds, straw, tree, and shrub branches) can be replaced by sheet materials with high tensile strength (Lukpanov, 2016). History of the development of domestic (meaning Kazakhstan) production of geosynthetic material began in the '70s–'80s of the last century when the Ministry of Transport Construction of the USSR issued a directive to expand their rational use in the construction of railways and roads (Ahmad and Mahboubi, 2021).

Today more than a 100 different types of geosynthetics are used in construction (Li *et al.*, 2018). The list of geosynthetic materials is expanding from year to year with new, more economical, and efficient materials. Geosynthetic material is mainly polymeric material, although sometimes rubber, fiberglass, and natural materials are used for its production (Hara *et al.*, 2010; Lin, 2013; Sato *et al.*, 2014; Dhanya and Divya, 2022).

As defined by American Society for Testing and Materials (2023a), a geosynthetic is a planar product manufactured from polymeric material used with soil, rock, earth, or other geotechnical engineering-related materials as an integral part of a man-made project, structure, or system.

The modern application of geosynthetics in construction is very wide, as well as a wide range of functional uses (Zhang, Javadi and Min, 2006; Abdelkrim and Buhan de, 2007; Zomberg, 2007; Chen *et al.*, 2012; Jiang, 2013). Thus, geosynthetic material can be used in retaining walls, foundations (soil basement),

pavements, and of course, in the structures of soil embankments (El-Naggar, Kennedy and Ibrahim, 1997; Ding and Hargrove, 2006; Wang, Chen and Gao, 2014; Kumar and Roy, 2022). The last one represents a mechanically stabilised earth (MSE) (Kanchi, Neeraja and Babu, 2015). This geotechnical structure will be discussed in this article together with the functional feature of using geosynthetics as a reinforcement element.

The article deals with the issue of assessing the stability of the soil dam (hereinafter embankment) of the ash-storage collector (ASC) of the thermal power plant of TPP1, a metallurgical plant in Temirtau (Kazakhstan). The ASC requires proper control, being the objects of increased danger. However, these geotechnical structures periodically exhaust their operational life, being subjected to irreversible deformations as a result of loss of stability. The latter leads to severe consequences, disruption of the normal operation of the power plant, as well as significant pollution of the environment (Lukpanov and Awwad, 2019).

During the period of operation, periodic investigations of the collapsed embankments and their monitoring were carried out with an assessment of the root causes of their emergency condition. According to the technical conclusions of experts, the main cause of embankment collapse was the geological structure of the dam foundation, which during wetting (in autumn and spring periods) significantly reduces its strength and deformation properties.

Despite the frequency of embankment collapses, no solutions were taken to eliminate the root causes of their occurrence. According to regulations, after each collapse, measures were taken to build up the embankment by backfilling, on the side of the collapsed slope. The measures undoubtedly included preventive technical solutions, such as installing additional drains, relocating water lines, reinforcing the downstream slope with dense masses, etc. Despite this, there was no significant result in eliminating the problems associated with embankment collapse.

The urgent issue of embankment stability caused the need to find a technical solution, which can be found in the use of geosynthetic reinforcement materials. As stated earlier, this technological solution is confirmed by deep world experience but requires localised approbation. Therefore, this article considers the evaluation of this technological solution for the stability of the embankment.

The goal of the study is to assess the effect of reinforcement elements on the stability of the soil embankment.

To realise the goal, the following tasks were carried out:

– conducting model (scaled) tests of the soil embankment;
– conducting numerical analysis of the soil embankment.

In both cases, two comparable variants were considered: a soil embankment with reinforcement elements and a soil embankment without reinforcement.

Model tests are to some extent natural, despite some conditions and assumptions (e.g., selection of equivariant materials with correction of physical and mechanical characteristics in proportion to the scale of the model, based on dynamic similarity). The obtained results of the stress–strain state of models have relatively high reliability; however, the technological process of model test production is very time-consuming. In this connection, the research work raised the question of assessing the reliability of the numerical method. If corrective factors can be obtained in the research process, the process of variational design can be accelerated because the simulation of different design situations by the numerical method is less time-consuming compared to model tests.

MATERIALS AND METHODS

The main research methods were:
– model tests (scaled tests);
– numerical simulation in the software Plaxis 2D.

Model tests. Model tests were performed in a sheet with sidewalls arranged at an angle (Fig. 1). The sheet has been made of a steel sheet, 0.8 cm thick. The maximum diameter of the sheet, with a maximum opening of the sidewalls, is 104 cm. The displacement of the walls is regulated by a screw, whereby a full turn of the screw is a transform of 1 mm of absolute displacement. The displacement increment (ε) is 0.1%, the maximum displacement is limited either by the maximum displacement of the sheet (12 cm) or by the collapse of the embankment.

Model tests had been made at a scale of 1:30. Radially moving elements of the sheet allow simulating the movement of soil masses, as a result of their leaching. Thus, not the process of leaching itself is simulated, but its consequence – the movement of soil masses – resulting in the loss of embankment stability (Fig. 2).

The embankment and subgrade were made of the same material, equivalent to the material of the full-scale embankment. There was no need to simulate the soil base (foundational soil) since in this formulation of the problem we considered the stability of the soil embankment itself, without evaluating the bearing capacity and stability of the soil base.
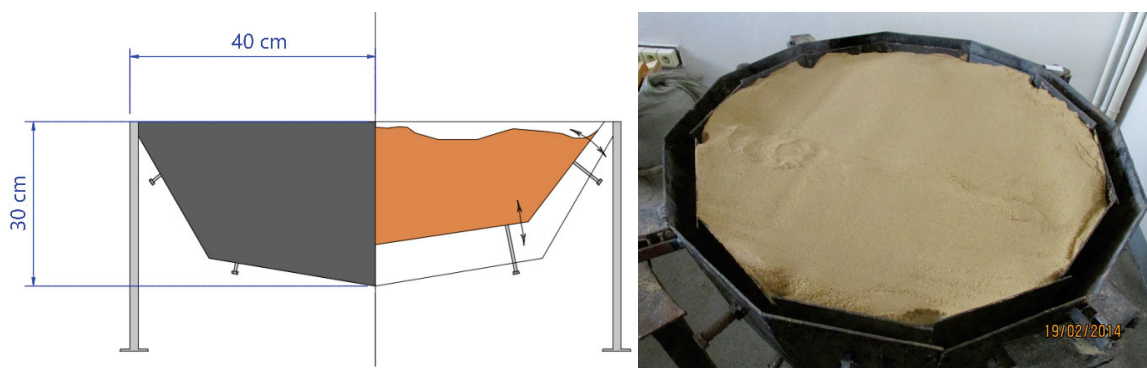

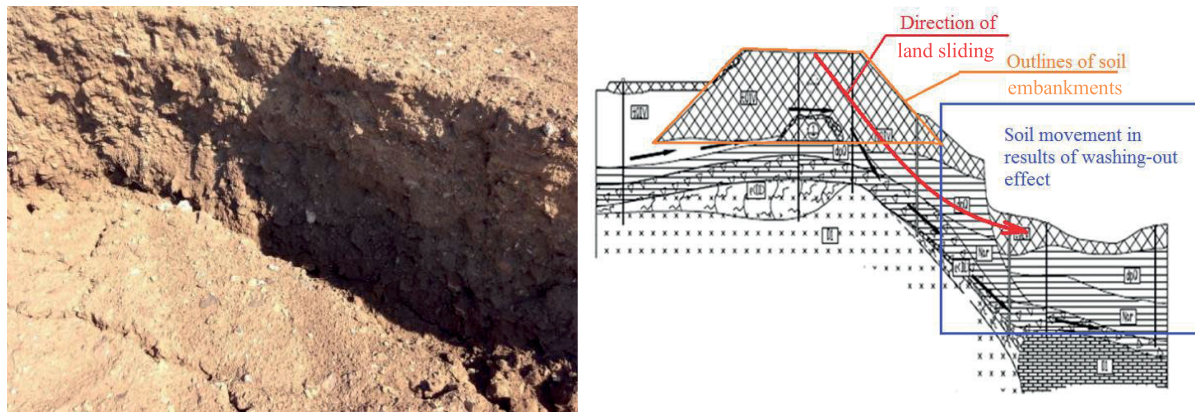Fig. 1. Design of metal radial sheet; source: own elaboration; photo of the metal radial sheet by *R.E. Lukpanov*

Fig. 2. Calculation model for loss of embankment stability; source: own elaboration; photo of the metal radial sheet by *R.E. Lukpanov*

Base and embankment fabrication was performed by layer-by-layer compaction of the equivalent layer: compaction with an impact load of each laid layer of soil, 5 cm thick (Photo 1a). Compaction was performed with density control by weighing the selected soil bunker (Photo 1b) to a specified unit weight of equivalent soil equal to 17 kN·m^{-3}. The dimensions of the model embankment were: a height of 25 cm, a width of the upper base of 17 cm, a width of the lower base of 40 cm, and a slope angle of 65° (which corresponds to the height of 7.5 m of the full-scale embankment with a width at the base of 12 m). Geogrid reinforcement, aperture 0.5 × 0.5 cm, was made in 3 rows, at 6, 12, and 18 cm height, (Photo 1c). The vertical deformation of the embankment was measured using Vibro+ measuring equipment installed on the top base of the embankment (Photo 1d). To assess the nature of the embankment deformation and to numerically control the deformation, markers installed on the soil base, the upper base of the embankment (Photos 1d, 1e), and the embankment slopes (Photo 1f) were used. A total of three experiments were conducted to mutually exclude one indicator from the three (if necessary).

Figure 3 shows the locations in the section and the plan, relative to which the comparative analysis will be made. In the flat formulation of the problem we were interested in the section perpendicular to the side face (four locations), in which three points for each of the locations were determined: at the foot (lower base) of the embankment (point A), at the cross (upper base) of the embankment (point B), at a distance from the foot, at 10 cm or 3 m of the natural dam (point C), and along the slope of the embankment at 10 cm from the foot or 3 m of the natural dam (point D).

The materials used in the model tests (embankment and soil base) have been on the basis of the general law of dynamic similitude, taking into account gravity and internal stresses.
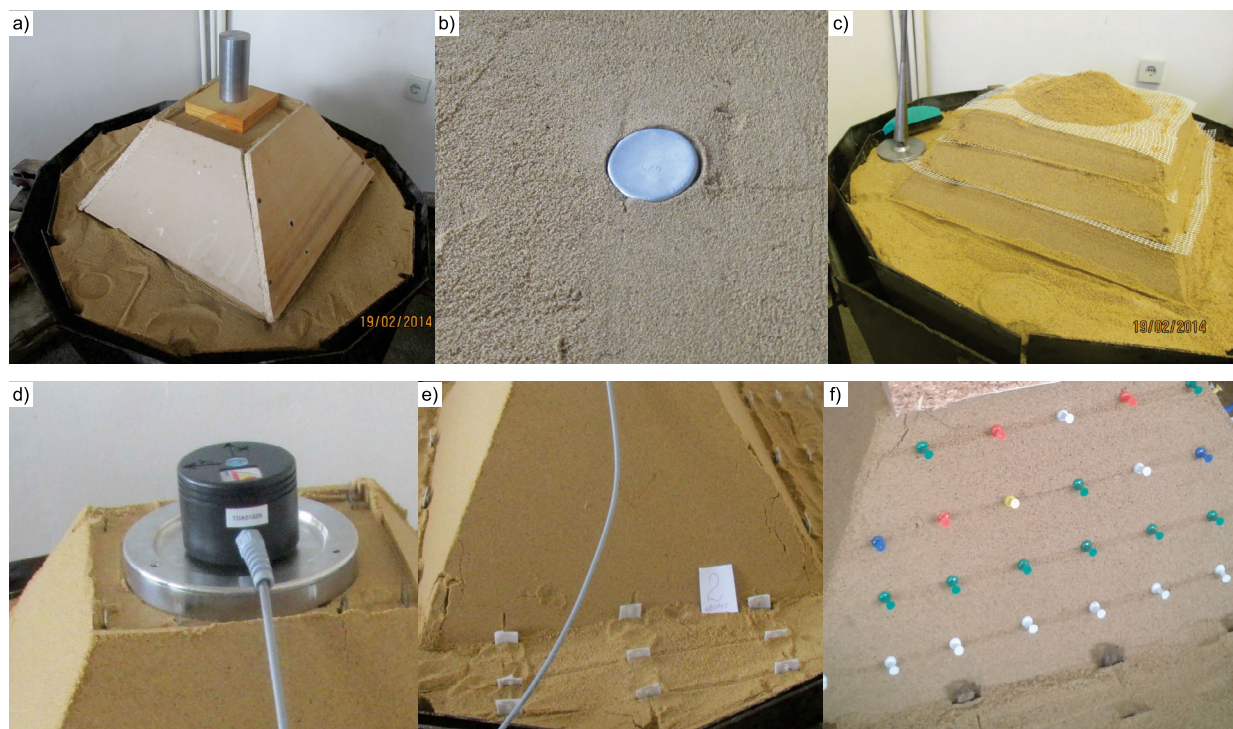

Photo 1. Model tests of the soil embankment: a) embankment formwork, b) density control, c) embankment installation, d) displacement transducer, e) bench marks, f) bench marks (phot. *R.E. Lukpanov*)
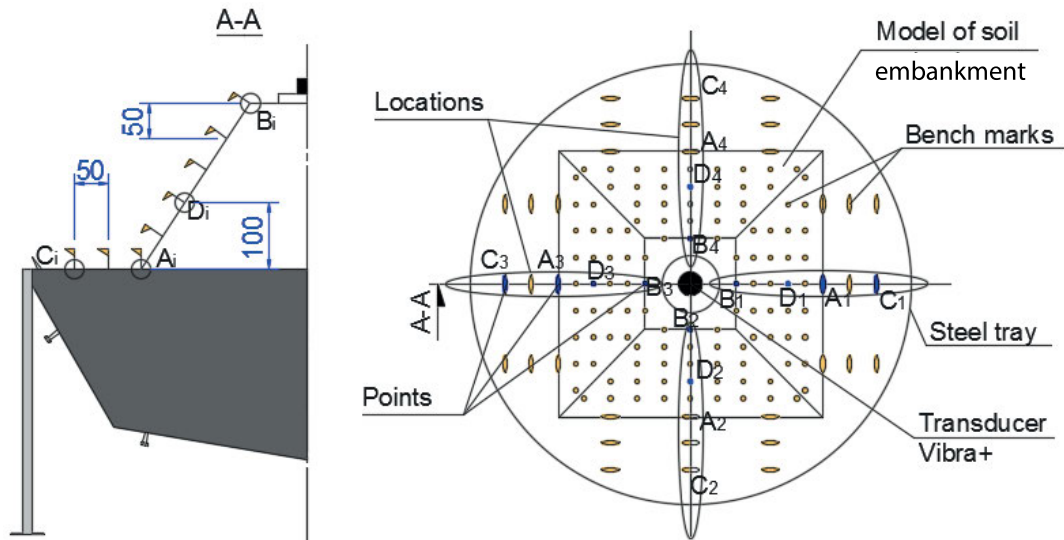
Fig. 3. Locations of points for comparative analysis; source: own elaboration

$$\frac{N_m}{\gamma_m I} = \frac{N_r}{\gamma_r J} = K = inv \qquad (1)$$

where: K = similarity (modelling) criterion; g_m, g_r = unit weight of model and real (full-scale) soil (m = model parameter, r = real parameter); I, J = linear dimensions of model and full-scale embankment; N_m, N_r = value corresponding to different characteristics (transformed by scale); inv = stress–strain relationships.

Equation (1) is converted to the Equation (2), by which the strength and deformation characteristics of equivalent materials had been at selected:

$$N_m = \frac{I}{J} \cdot \frac{\gamma_m}{\gamma_r} \cdot N_r \qquad (2)$$

Knowing the parameters of the modelled objects, as well as the scale of modelling, equal to 1:30, we calculate the required parameters of the equivalent material (Tab. 1).

To determine the axial stiffness of the model reinforcement elements, we will use the law of dynamic similarity for 1 m of the natural dam or $\frac{1}{30}$ m of the modelled dam. According to the results of tests of natural geogrid, it was obtained: tensile forces of one rod of geogrid at 2% stretching are, on average, 26.96 MN·m^{-2}, and the coefficient of variation was 3.85%.

Thus, the axial stiffness of the model reinforcement element (with the density of natural geogrid 9.5 kN·cm^{-2} and the density of the equivalent reinforcement material 7.4 kN·cm^{-2}) is EA (normal stiffness) = 0.36 kN·m^{-1}. That is, the strip of equivalent material, width of 3.3 cm, must withstand a load

Table 1. Parameters of soil and equivalent material

Parameter	Soil	Equivalent material	
Unit weight of soil (kN·m^{-3})	16	17	–
Unit weight of wet soil (kN·m^{-3})	18	20	–
Soil deformation modulus (MPa)	18	0.64	$E_m = \frac{I}{J} \cdot \frac{\gamma_m}{\gamma_r} \cdot E_r$
Specific soil cohesion (kPa)	7	0.25	$C_m = \frac{I}{J} \cdot \frac{\gamma_m}{\gamma_r} \cdot C_r$
Angle of internal friction of soil (°)	23	20	$\varphi_m = \varphi_r$
Dilatancy angle of soil (°)	0.0	0.0	$\psi_m = \psi_r$
Poisson's ratio of soil	0.35	0.35	$v_m = v_r$
Permeability in the lateral direction of soil (m^3·d^{-1})	0.001	0.1	–
Permeability in the vertical direction of soil (m^3·d^{-1})	0.001	0.1	–

Explanations: E_m, C_m = deformation modulus and cohesion of the equivalent material, E_r, C_r = deformation modulus and cohesion of real soil, φ_m = internal friction angle of the model soil, φ_r = internal friction angle of the real soil, ψ_m = dilatancy angle of the model soil, ψ_r = dilatancy angle of the real soil, v_m = Poisson's ratio of the model soil, v_r = Poisson's ratio of the real soil.
Source: own study.

weighing of 367 N. As a reinforcement element, a geosynthetic mesh made of polyester, with a pitch of 0.5 cm, was used. According to the test results of the mesh fibres of the equivalent reinforcement element, the tensile strength ranges from 87 N to 115 N, which satisfies the aforementioned tensile strength requirements.

Numerical modelling. Numerical simulations were performed in Plaxis 2D software. The simulation of the flume test itself, rather than the computational situation of a real soil embankment, was carried out. This paper presents preliminary studies that aim to assess the validity of the numerical simulation results and, therefore, to evaluate its reliability as a research method. Validation of the method is performed in comparison with the results of model tests.

Numerical modelling was performed in two problem statements:
– task 1: simulate model tests using the characteristics of equivalent material at a real scale of the sheet;
– task 2: Simulate model tests using real soil characteristics at the real scale of the soil embankment of the ash-storage collector (ASC).

Once the first stage is completed, the evaluation will be done by comparing the results of the numerical simulation and the small-scaled model test. In the first stage, we obtain the correction factors we need to adjust the results of the numerical simulation relative to the modelled (but still *in situ*) test. Once the second step is complete, the evaluation will be done by comparing the results of the numerical simulation of the model test using an equivalent layer (step 1) and the numerical simulation of the same model test, but at a larger scale of 1:30 using real soil. In step 2, we will obtain correction factors of the results of the numerical simulation relative to the full-scale embankment. Thus, we can change the geometry and design situations of the soil embankment in the numerical simulation, followed by a correction to the results.

The geogrid is modelled in the Plaxis 2D software using the "Geotextile" command, which specifies a single parameter – the normal stiffness. Thus, the flat object of the numerical simulation only accepts axial tensile forces and cannot accept compressive forces.

Since the computational situation is considered in the plane strain, the *EA* will be determined from the tensile strength (*F*) of the 1 m wide geogrid (Fig. 4). The tensile strength value was obtained by tensile machine tests for one rod, so the normal
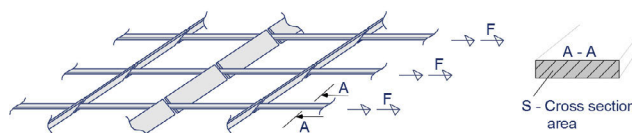

Fig. 4. Geogrid geometry; *F* = tensile strength; source: own elaboration

stiffness specified in the numerical simulation was determined as follows:

$$EA = \sigma_t \cdot S \cdot n \qquad (3)$$

where: EA = normal stiffness (kN·m^{-1}), σ_t = tensile strength of one geogrid rod (kN·m^{-2}), S = the cross area of the geogrid rod (m^2), n = number of rods in a 1 m wide geogrid (m^{-1}).

For the studies presented in this article, a set of tests for the evaluation and selection of materials was carried out:
– natural geogrid grab (tensile force) tests (Photo 2a);
– equivalent geogrid grab (tensile force) tests (Photo 2b);
– pull-out tests of full-scale geogrid on the equivalent soil (Photo 2c).

Within this article, the final technical solutions will be given, with a brief description of the methods that contribute to their adoption.

Tests to assess the tensile strength of the geogrid were conducted according to the requirements of the standard ASTM D6637/D6637M test method for determining tensile properties of geogrids by single or multi-rib tensile method (American Society for Testing and Materials, 2023b). Based on the tests, the axial stiffness of the reinforcement element EA = 14.0 kN·m^{-1} (at a geogrid pitch of 5 cm, 1 × 5 mm cross-section) was accepted for a plane strain in Plaxis 2D. To determine the axial stiffness of the model reinforcement elements will use the law of dynamic similarity per 1 m of the natural dam or $\frac{1}{30}$ m of the modelled dam. Polyester geosynthetic mesh with 0.5 cm spacing was used as a reinforcement element. The fibre strength of the model geogrid was determined on a TMA-1000 thermomechanical analyser test equipment designed for testing the thermal and mechanical characteristics of small samples. The main evaluation criterion was to meet the requirements of axial stiffness of 360 kN·m^{-1} and more.

Numerical estimation of interface values was performed by laboratory pullout tests of geogrid from the soil mass. Determination of the interface coefficient value was performed using the following formula:
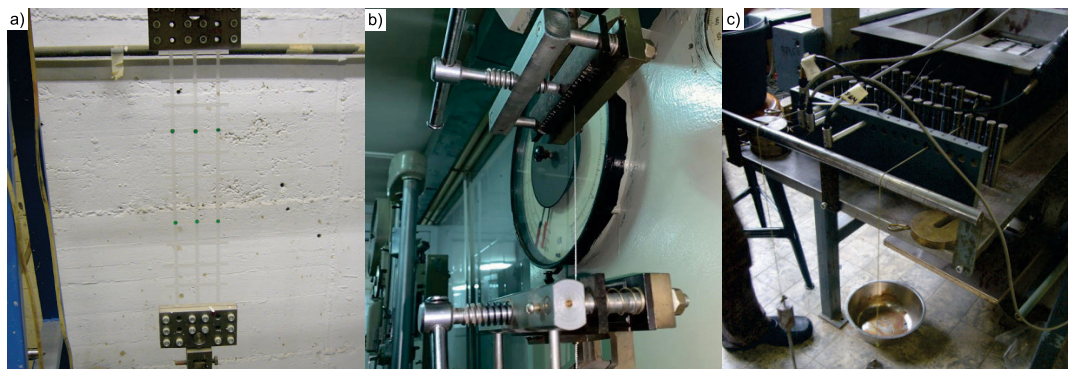

Photo 2. Preliminary tests of the geogrid: a) tensile strength of natural geogrid, b) tensile strength of equivalent ribs, c) pull out test of geogrid (phot. *R.E. Lukpanov*)

$$R = \frac{F_{pt}}{\sigma_t \cdot s} = \frac{F_{pt}}{F_t} \qquad (4)$$

where: R = lowering factor (kN·m^{-1}), σ_t = tensile strength of geogrid (kN·m^{-2}), F_{pt} = pulling force (kN), s = the cross area of geogrid rods (m^2), F_t = the maximum carrying capacity of the geogrid reinforcement material under tensile stress. With a sample width of 30 cm, the number of rods is 7 pieces. Then the maximum carrying capacity of the material is

$$F_t = \frac{7 \text{ rods} \cdot 70 \text{ MPa} \cdot 10^6 \left(1 \cdot 10^{-3} \cdot 5 \cdot 10^{-3}\right)}{9.81} = 250 \text{ kgf} = 2.45 \text{ kN}$$

Thus, the tensile resistance (during embankment deformation), will not be limited by the maximum tensile strength of the geogrid, but by the soil resistance when the geogrid is pulled out (Photo 2c). That is, the maximum tensile strength of the geogrid will correspond to the failure of material continuity, while the loss of overall embankment stability will correspond to the soil's resistance to geogrid pulling out.

When designing it would have been rational to use exactly the linear resistance figure, but for the decreasing interface factor, it was decided to use the average of the three received resistance values, equal to 1.602 kN or 163.3 kgf. So the interface factor is R = 163.3 : 250 = 0.65.

In Figure 5, the design scheme of the (a) reinforced and (b) unreinforced model of the embankment in the Plaxis 2D software, performed in the Coulomb–Mohr plane strain model is depicted. To make it relatively difficult to simulate the operation of the sheet, the following solution was adopted – the sheet model was placed in weakly compressible soil. The last one is explained by the complexity (or even limitation) of setting the boundary conditions for the sheet of complex geometry, with the possibility of prescribed displacement of the boundaries. That is, the program does not provide such a problem statement, so it was decided to place the sheet in ground conditions, followed by a prescribed displacement of the sheet walls (Fig. 5). In such a case, the boundary dimensions of the plane model and the soil parameters around the sheet are stipulated by their potential compressibility until the model test walls are completely displaced. The generation of the finite element mesh of the model outside the sheet is done on a large scale and within the sheet on a small scale. This is because the stress–strain state of the soil outside the sheet is not considered, the external soil mass is required only to simulate a given displacement of the inclined walls of the sheet.

RESULTS AND DISCUSSION

Model scaled test. The results of the model tests are shown in Figures 6–8. The results are represented by the dependencies between the given prescribed foundational soil displacement (caused by the displacement of the sheet side walls) and the embankment deformations (vertical and lateral), and the resulting (total) deformation. The relationships between the prescribed displacement and the vertical deformations of all locations and points for the reinforced embankment are shown in Figure 6a. The same relationships for an unreinforced embankment are shown in Figure 6b. The relationships between the prescribed displacement and lateral deformations for the reinforced embankment are depicted in Figure 7a, and in Figure 7b, the same relationships for the unreinforced embankment are shown. The relationship between the prescribed displacement and the resulting deformation for the reinforced embankment is presented in Figure 8a, and in Figure 8b, for the unreinforced embankment.

The deformation parameters of the reinforced embankment and the unreinforced embankment are compared in Figure 9. Comparisons of absolute values of vertical deformations are shown in Figure 9a, comparisons of lateral deformations – in Figure 9b, and comparisons of resultant deformations – in Figure 9c. The solid line shows the absolute values and the dashed line shows the trend lines. In Figure 10, the contours of the maximum deformed embankment and foundation with and without reinforcement are shown. A scale of 1:5 was used for visualisation.

The visual effect of reinforcement can be seen when comparing the deformation contours of the embankments. Even when scaled up by a factor of five, the deformation of a reinforced embankment is not significant relative to an unreinforced embankment, even though the displacement of the underlying soil is palpable in both cases.

According to the results of model tests, the values of deformability of the soil embankment during the movement of the underlying soil base were obtained. The maximum deformation values were obviously observed at points C, i.e., at locations as close as possible to the origin of displacement (or a prescribed displacement), and the minimum values at points B or locations as far away from the origin as possible. The vertical maximum deformation of the foundational soil base in the case of the unreinforced model ranged from 10.9 to 11.7 mm, with an average value of 11.4 mm. In the case of the reinforced
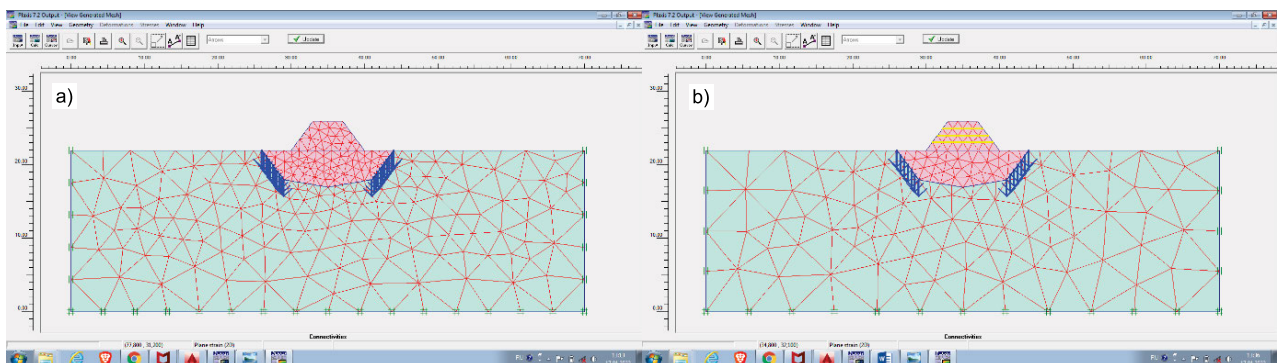

Fig. 5. Design scheme of the embankment model: a) modelling of unreinforced embankment, b) modelling of reinforced embankment; source: own elaboration
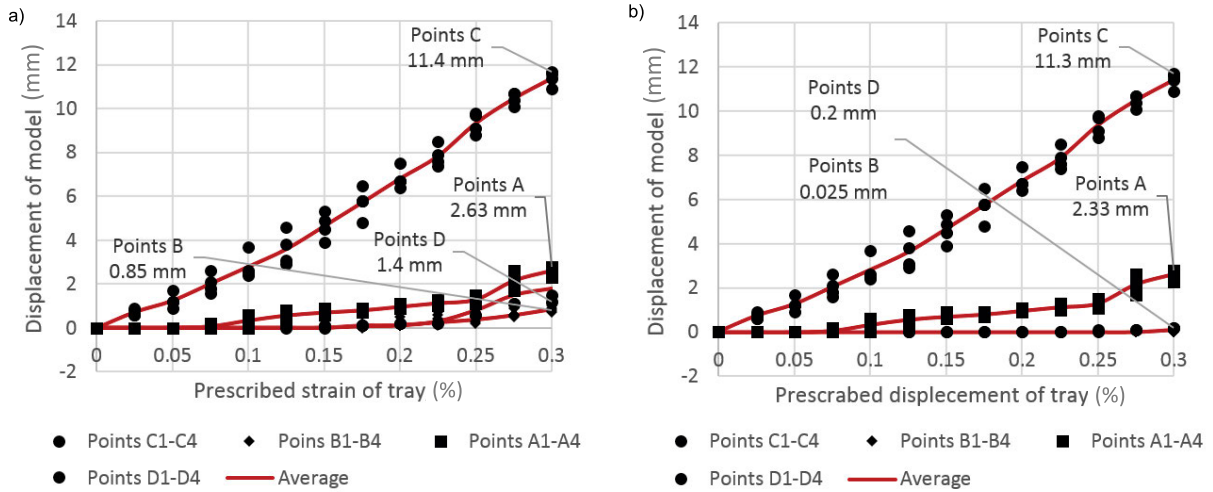
Fig. 6. Dependence between the prescribed displacement and vertical deformations: a) reinforced embankment, b) unreinforced embankment; source: own study
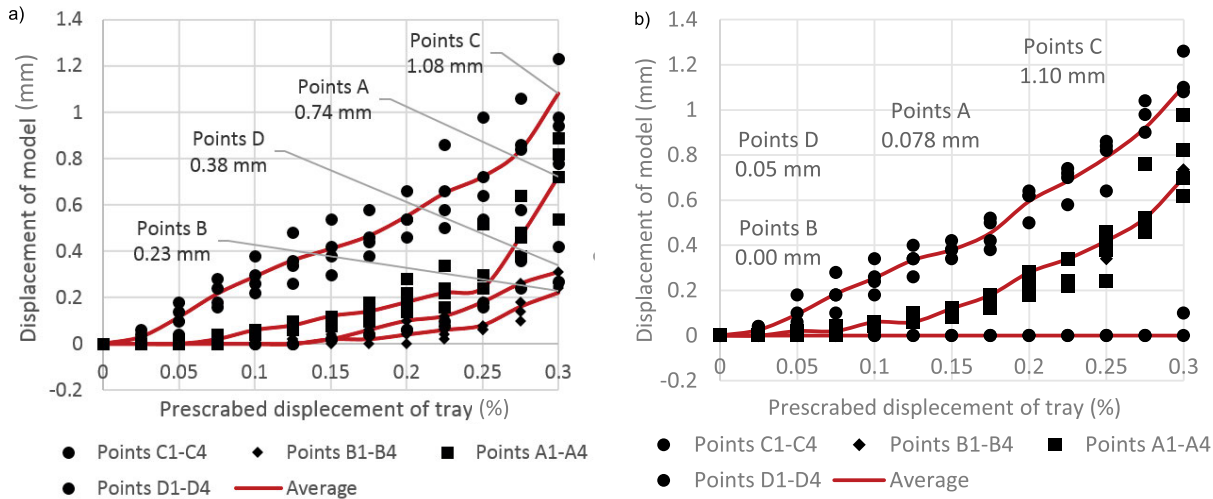

Fig. 7. Dependence between the prescribed displacement and lateral deformations: a) reinforced embankment, b) unreinforced embankment; source: own study
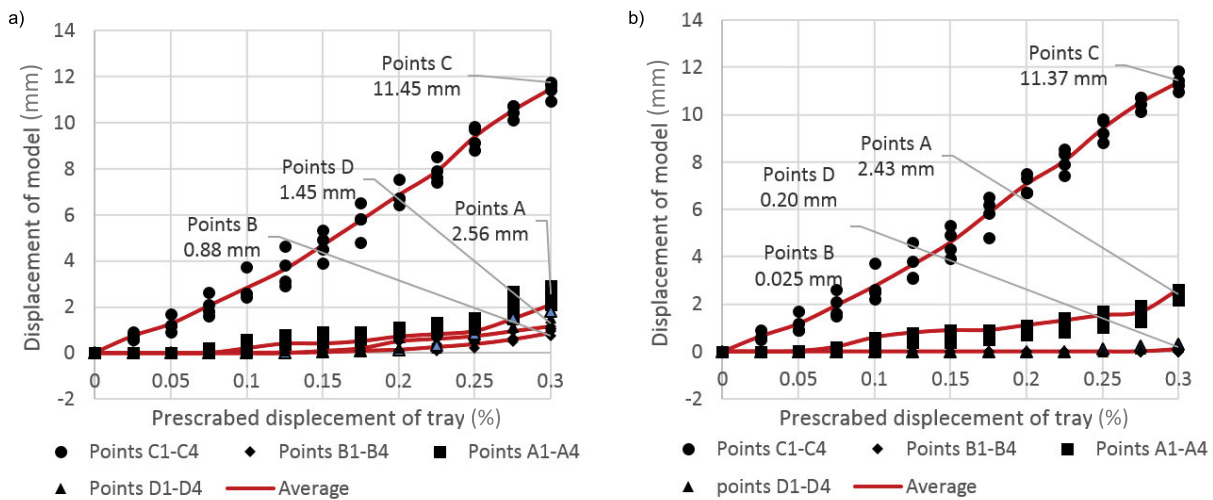

Fig. 8. Dependence between the prescribed displacement and the resulting deformations: a) reinforced embankment, b) unreinforced embankment; source: own study
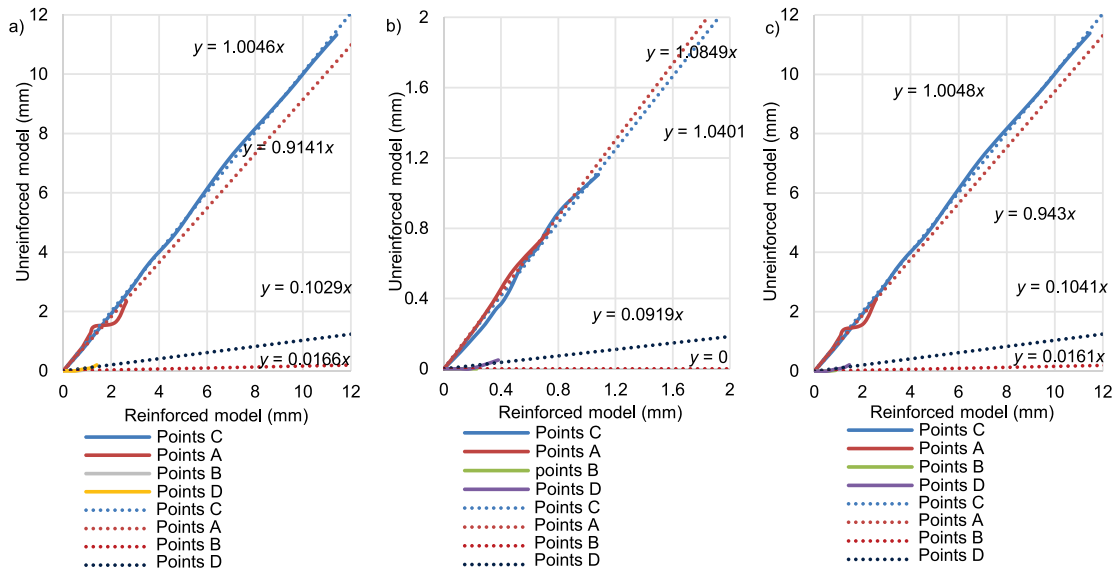
Fig. 9. Comparisons of deformation of reinforced and unreinforced embankments: a) vertical deformation, b) lateral deformation, c) resultant deformation; source: own study
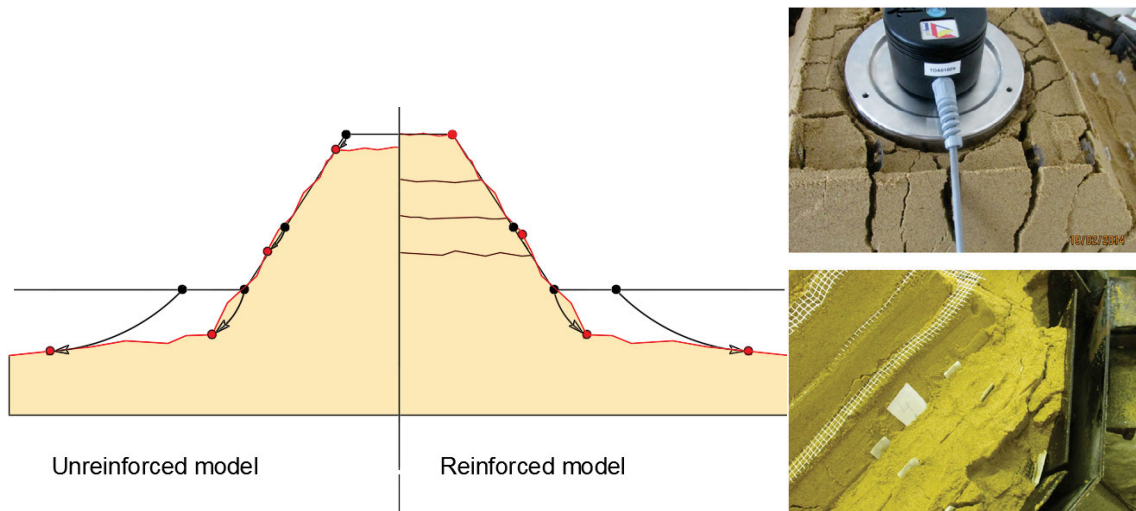

Fig. 10. Deformation of the reinforced and unreinforced embankment; source: own study; photos of the embankment models by *R.E. Lukpanov*

embankment, the same values ranged from 10.9 to 11.8 mm, with an average value of 11.35 mm. The lateral maximum deformation of the unreinforced model ranged from 0.68 to 1.46 mm, for the reinforced 0.98 to 1.26 mm, with average values of 1.08 and 1.10 mm (for the unreinforced and reinforced model, respectively). In both cases (reinforced and unreinforced embankment) maximum similar values were obtained, there were very close deformation manifestations of the models, as evidenced by the values of the resulting deformations: unreinforced model, in the range of 10.94–11.79 mm, average 11.45 mm; reinforced – of 10.95–11.87 mm, average 11.38 mm.

Smaller than in point C, but still high values of vertical deformations were observed in points A – locations at a lateral distance of 10 cm from the source of the prescribed displacement. For the unreinforced model, the maximum lateral deformations range from 1.9 to 2.8 mm, and for the reinforced model – from 2.1 to 2.5 mm. All obtained values have a close relationship, with average values of 2.45 and 2.30 mm (for the unreinforced and reinforced models, respectively). Lateral deformations range from

0.58 to 0.96 mm for the unreinforced model and from 0.62 to 0.98 for the reinforced model. The average values also have a high convergence and are 0.74 and 0.78 mm (for the unreinforced and reinforced models, respectively). The resulting deformations range from 2.03 to 2.96 mm for the unreinforced model and from 2.19 to 2.63 mm for the reinforced model. The average values are 2.56 mm for the unreinforced model and 2.43 mm for the reinforced model. The high convergence of the deformation values has a logical pattern and can be explained by similar model conditions in both cases, without reinforcement of the soil base.

Insignificant ground displacement was observed at point D, located on the slope of the embankment. The maximum vertical deformations of the unreinforced model range from 1.1 to 1.8 mm, while the same values for the reinforced model are only 0.1 to 0.3 mm. With average values of 1.4 and 0.2 mm (for the unreinforced and reinforced model, respectively), the effect of reinforcement is a sevenfold reduction in deformation in the vertical direction, and the vertical deformation of the embankment base is 11 times greater than the deformation of the

reinforced slope. The lateral deformation of the unreinforced model ranges from 1.7 to 2.2 mm (average 1.9 mm), and that of the reinforced model from 0.0 to 0.1 mm (average 0.05 mm). In this case, the effect of reinforcement is a sevenfold reduction in lateral deformation, and the slope deformation is 16 times less than the base deformation of the embankment. The total deformation respectively has a large difference between the reinforced and unreinforced model: the unreinforced model is between 1.15 and 1.83 mm, with an average value of 1.45 mm; the reinforced model is within 0.10–0.31 mm, with an average value of 0.20 mm. The total deformation reduction from reinforcement is 90%, and the total slope deformation is 11 times less than the total base deformation of the embankment.

The minimum deformation values were observed at the location of the embankment crest, at points B. The maximum vertical deformations of the unreinforced model range from 0.7 to 1.0 mm, with an average of 0.85 mm, while the same deformation values for the reinforced model are from 0.0 to 0.1 mm, with an average of 0.025 mm. In this location, the effect of reinforcement is reflected in a 34-fold decrease in vertical deformation, and a 92-fold decrease relative to the deformation of the underlying foundational soil base. The maximum lateral deformations of the unreinforced model range from 0.16 to 0.28 mm, with an average value of 0.23 mm, while the lateral deformations of the reinforced model were not detected. Consequently, in this case, the maximum effect of reinforcement with a high degree of stability of the embankment crest was obtained. Comparisons of the total deformation values showed the following: unreinforced model in the range of 0.71–1.04 mm, with an average value of 0.88 mm; reinforced model in the range of 0.0–0.1 mm, with an average value of 0.025 mm. Thus, the maximum effect of reinforcement concerning stability is 97.3% (relative to the underlying soil base). The ratio of the reduction of the total deformation relative to the unreinforced model is 35 times, and relative to the underlying base is 97 times.

The analysis of the statistical parameters of the obtained results indicates a close relationship of individual values. The obtained coefficients of variation within locations do not exceed 15%, which confirms the reliability of the obtained results, the research method and the identified patterns.

The effect of reinforcement elements on the reduction of embankment deformation can be observed in the comparative graphs of Figure 9. The presented regularities or, more precisely, the equations show the degree of influence of reinforcement: the closer the argument variable "x" to 1, the less the reinforcing effect appears, and vice versa, the greater the difference between the argument variable "x" from 1, the greater the effect of reinforcement on embankment stability.

A significant influence of reinforcement is observed at location B, where the variable vertical strain is 0.0166, the lateral strain is 0, and the total strain is 0.0161. A relatively smaller, but also significant influence is detected at location D: the variable vertical strain is 0.10, the lateral strain is 0.09, and the total strain is 0.10. Obviously, the minimum influence was detected at locations A and C, where no reinforcement was provided: the vertical deformation variable is 1.004 and 0.9141, respectively, lateral – 1.04 and 1.08, and total – 1.004 and 0.944.

Numerical modelling. Task 1. The maximum vertical displacements in both cases (unreinforced and reinforced embankment) are observed at point C, which is obvious because this location is close to the source of the prescribed displacement.

The maximum displacement values are: for unreinforced embankment – 11.72 mm, for reinforced embankment – 11.53 mm. Relatively smaller vertical displacements, also similar in both cases, were observed at point A: 3.11 mm for the unreinforced embankment and 2.79 mm for the reinforced one. The similarity of the deformed state of the subgrade of the reinforced and unreinforced embankment is logical since the reinforcing effect does not extend to the subgrade. The maximum reinforcing effect was detected in the embankment crest (location B). The difference in vertical displacement of unreinforced embankment was 24 times greater than that of reinforced embankment: vertical displacement of unreinforced embankment was 1.48 mm, and reinforced embankment – 0.06 mm. Relatively less reinforcement was found on the slope (location D). The difference in vertical displacement relative to the reinforced embankment was 4.5 times: vertical displacement of the unreinforced embankment – 1.72 mm, and reinforced – 0.38 mm.

A similar relationship was observed when comparing lateral displacements. The displacements at location C for the unreinforced embankment were 1.87 mm and for the reinforced embankment – 1.35 mm. The displacements at location A were 1.05 and 1.02 mm for unreinforced and reinforced embankments, respectively. The maximum difference in lateral displacement between unreinforced and reinforced embankments at location B is 12 times: lateral displacement of unreinforced embankment being 0.24 mm, reinforced – 0.02 mm. The smaller difference corresponds to location D and is also 12 times: 0.79 mm for unreinforced and 0.064 mm for reinforced embankments.

The total displacements at location A were 3.25 and 3.76 mm for unreinforced and reinforced embankments, respectively. The total displacements at location C were 11.89 mm for unreinforced embankment and 11.74 mm for reinforced embankment. For location D, the displacements were 1.73 mm and 0.43 mm for unreinforced and reinforced embankments, respectively, with a fourfold reduction in total displacement as a result of embankment reinforcement. For location B, where the maximum effect of reinforcement is observed, the displacements were 0.49 and 0.07 mm for unreinforced and reinforced embankments, respectively, with a sevenfold reduction in total displacement.

In Figures 11 and 12, there are diagrams comparing the sheet test displacements and numerical simulation results of task 1 for the unreinforced and reinforced embankments, respectively. The abscissa axis (conventionally named variation) shows different locations of benchmarks during model tests, and the ordinate axis respectively shows their displacements. In Figure 11a, there are comparisons of vertical displacements, in Figure 11b – comparisons of lateral displacements, and in Figure 11c – the total displacements of the unreinforced embankment. In Figures 12a, 12b, and 12c, there are the same comparisons for the reinforced embankment.

The difference of vertical and lateral displacements, as well as the average values of different locations of model tests and numerical modelling, are shown in Table 2.

According to the comparison results, the average values of the total displacements in location A of the unreinforced embankment of the model test were 2.56 mm, whereas the same values in Plaxis 2D were 3.25 mm. The percentage difference was 26.9%. The average values of the total displacements of location C of the same values were 11.45 and 11.89 mm, the percentage
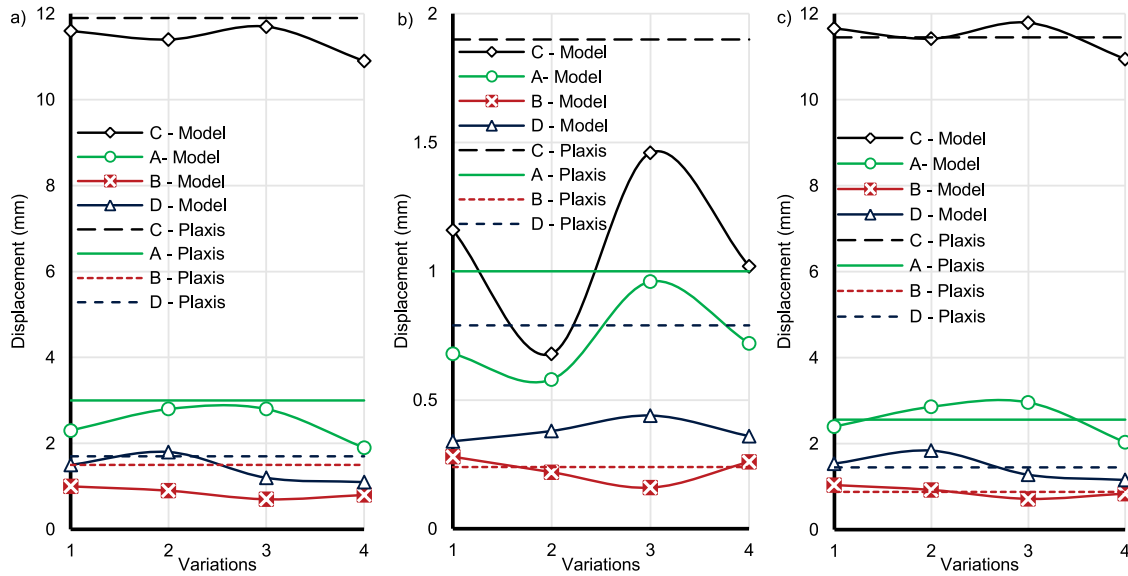
Fig. 11. Comparisons of model test results and numerical simulations of task 1 unreinforced embankment: a) vertical deformation, b) lateral deformation, c) resultant deformation; source: own study
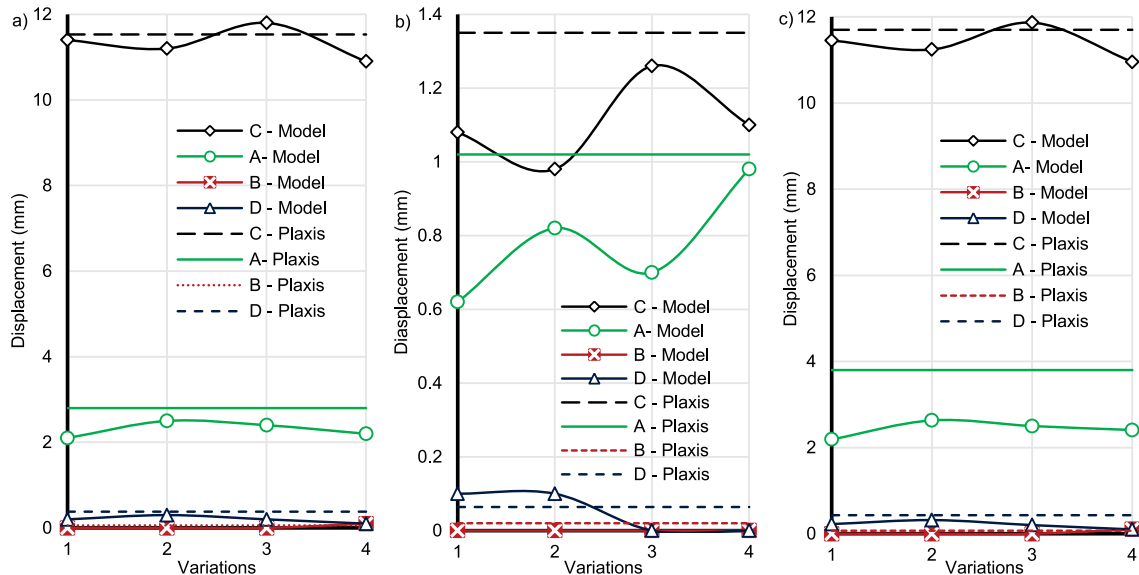
Fig. 12. Comparisons of model test results and numerical simulations of task 1 of the reinforced embankment: a) vertical deformation, b) lateral deformation, c) resultant deformation; source: own study

difference was 3.8%. The average values of location B of the same parameters were 0.88 and 1.58 mm, the difference in the percentage was 79.5%. For location D the difference was 19.3%. There is a tendency to increase the percentage difference in the data with the distance from the excitation source: if near the prescribed displacement (location C) the difference was on average 3.8%, then at the most distant point (location B) the difference averaged 79.5%. For the reinforced model, the difference in total displacements at location A was 54.7%, with average values of 2.43 mm (model tests) and 3.76 mm (Plaxis 2D). The difference in location C displacements was 1.3%, with average values of 11.58 and 11.74 mm, respectively. The difference in location B was 180% with the same values of 0.025 and 0.07 mm, respectively. For location D, the difference was 115% with values of 0.20 and 0.43 mm. In general, there is a similar tendency of increasing divergence with distance from

the prescribed displacement, with a more pronounced divergence at the reinforcement locations.

The resulting ratios shown in Table 2 can be taken as correction factors for vertical, lateral, and total displacements, depending on the distance to the source of a prescribed displacement or, in reality, on the displacement of the underlying foundational soil base. The data points of the diagram show the ratios of the deformation results of task 1 (numerical modelling) to the deformations of the model tests. Thus, by multiplying the numerical modelling results by the correction factor, we obtain the value of the model test deformation. The resulting correction factors can be expressed by the functions shown in Figure 13, where Figure 13a displays the correction factors for the unreinforced embankment, and Figure 13b – for the reinforced embankment.

Numerical modelling. Task 2. The results of calculations of task 2 are similar in the quality of deformation to task 1, but the

Table 2. Comparison of model test results and numerical modelling task 1

Location point	Vertical displacements (mm)			Lateral displacements (mm)			Total displacements (mm)		
	model (mm)	Plaxis 2D (m)	Plaxis 2D/ model	model (mm)	Plaxis 2D (m)	Plaxis 2D/ model	model (mm)	Plaxis 2D (m)	Plaxis 2D/ model
Unreinforced model									
C	11.4	11.72	1.03	1.08	1.87	1.73	11.45	11.89	1.04
A	2.63	3.11	1.18	0.74	1.05	1.43	2.56	3.25	1.27
D	1.4	1.72	1.23	0.38	0.79	2.08	1.45	1.73	1.19
B	0.85	1.48	1.74	0.23	0.24	1.04	0.88	1.58	1.80
Reinforced model									
C	11.32	11.53	1.02	1.105	1.35	1.22	11.58	11.74	1.01
A	2.33	2.79	1.20	0.78	1.02	1.31	2.43	3.76	1.55
D	0.2	0.38	1.90	0	0.06	–	0.2	0.43	2.15
B	0.025	0.06	2.40	0.05	0.02	0.40	0.025	0.07	2.80

Source: own study
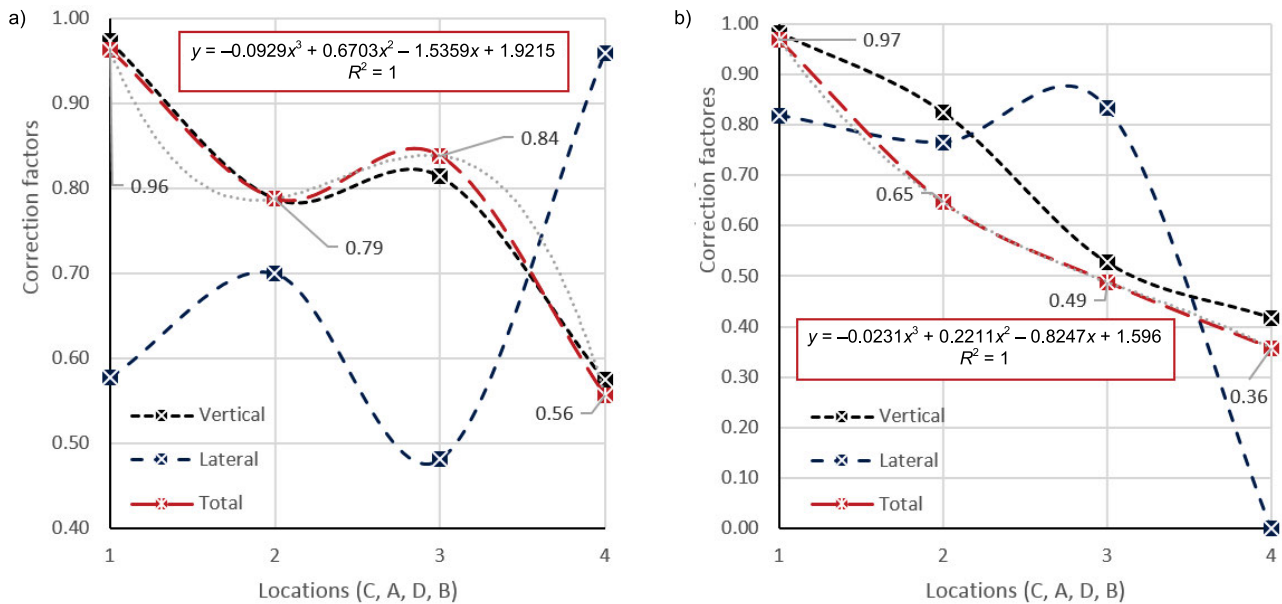
Fig. 13. Corrective factors of task 1 according to the results of model tests: a) reinforced embankment, b) unreinforced embankment; source: own study

quantitative values are different. The maximum absolute values of vertical displacements in both cases (unreinforced and reinforced model) at location C are 3.47 and 3.34 m, respectively, and the ratio of unreinforced to reinforced model (presented further) is 1.04. Smaller vertical displacements in location A are 2.62 and 1.62 m for unreinforced and reinforced models, respectively; the ratio is 1.61. The maximum difference of vertical displacements in location B is 24.02, with absolute values of 1.41 and 0.06 m for unreinforced and reinforced embankments, respectively. Relatively smaller but also significant difference in location D is 3.78, with values of 1.74 and 0.46 m, respectively.

A similar trend of ratios is revealed when comparing lateral displacements. Maximum values in location C, where the ratio is 1.11 with absolute lateral displacements of 0.68 and 0.61 m for unreinforced and reinforced models. The displacements at location A are 0.41 and 0.22 m, respectively, where the ratio is

1.85. The maximum ratio, which corresponds to the minimum values of displacements also in location B, is 25.63, with absolute values of 0.28 and 0.01 m, respectively. The ratio at location D is 10.92, with values of 1.36 and 0.04 m, respectively.

The total displacements also have a similar tendency. At location C, the ratio was 1.02 for total displacements of 3.54 and 3.47 m for the unreinforced and reinforced models, respectively. At location A, the ratio was 1.62, with displacements of 2.68 and 1.66 m, respectively. At location B, the ratio was 21.86, with displacements of 1.53 and 0.07 m, respectively. The ratio at location D was 3.83, with values of 1.85 and 0.42 m. In Figures 14 and 15, there are comparisons of the results of the numerical modelling of task 2 to task 1, the unreinforced and the reinforced model, respectively. The comparison of individual values of displacements is performed taking into account the scale of 1:30 models. In Figure 14a, the results of comparisons of vertical displacements of tasks are described, in Figure 14b – the
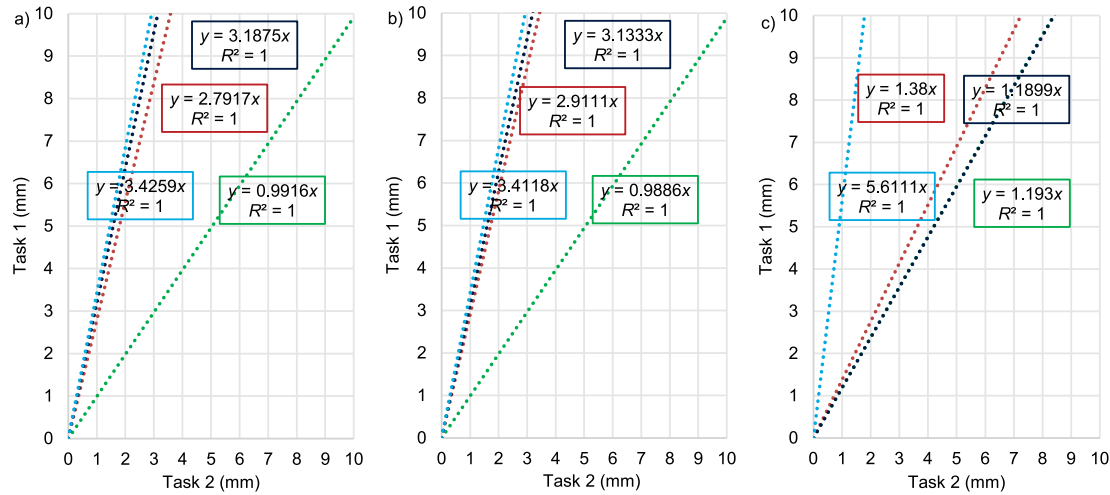
Fig. 14. Comparison of displacement results of unreinforced models: a) resultant deformation, b) vertical deformation, c) lateral deformation; source: own study
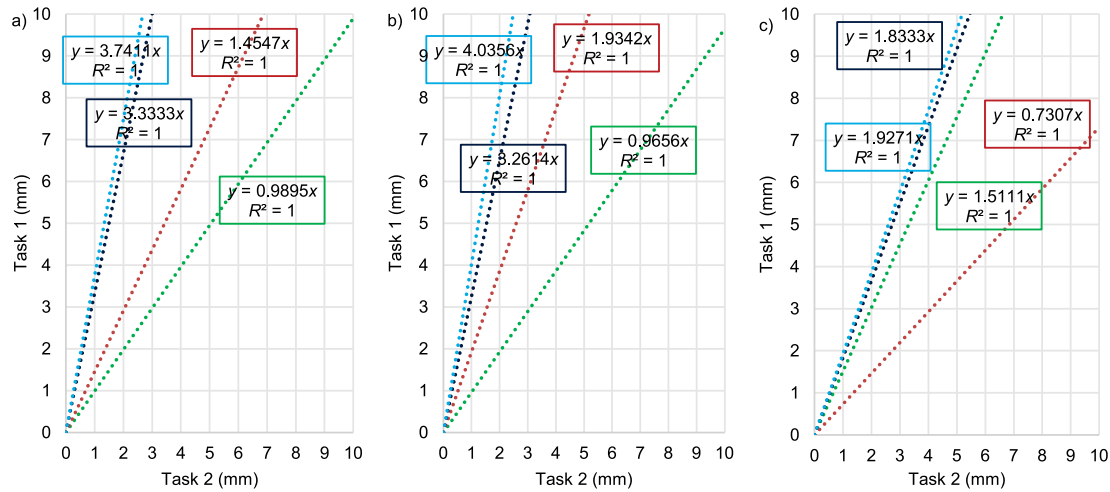
Fig. 15. Comparison of displacement results of reinforced models: a) resultant deformation, b) vertical deformation, c) lateral deformation; source: own study

comparisons of lateral displacements, and in Figure 14c – the comparisons of total displacements. In Figures 15a–15c, the comparisons of displacements of reinforced models in the same sequence are shown. The equations presented in the figures characterise the ratios of particular values of task 2 to task 1, which can be conventionally referred to as ratio coefficients.

According to the diagrams in Figure 14, the minimum ratio coefficients (for unreinforced embankments), which correspond to the maximum convergence of individual values, correspond to location C: for vertical the displacement is 0.99, for lateral – 1.19, and for the total – 0.99. The least convergence of individual values is observed at location A, where the ratio coefficients are: 2.91 for vertical displacement, 1.38 for lateral, and 2.79 for total. Even less convergence is typical for location D, the ratio coefficients are: for vertical displacement – 3.13, for lateral – 1.19, and for the total – 3.19. The minimum convergence corresponds to the maximum ratio coefficients revealed at location B: for vertical the displacement is 3.41, for lateral – 5.61, and for the total – 3.42.

A similar tendency is observed for reinforced embankments (Fig. 15). Maximum convergence is detected at location C, which corresponds to the following ratios: for vertical displacement, it is 0.96, for lateral displacement – 1.51, and for the total – 0.99. The

convergence of individual values of location A is expressed by the following ratio coefficients: for vertical displacement, it is 1.93, for lateral displacement – 0.73, and for the total – 1.45. The ratio coefficients at location D are: for vertical displacement, it is 3.26, for lateral displacement – 1.83, and for the total – 3.33. The correlation coefficients at location B are: 4.03 for vertical displacement, 1.93 – for lateral, and 3.74 for the total.

In Figure 16, the correction factors are shown that allow to correct the deformation of the embankment contour along the slope and underlying base (locations A–D) obtained by numerical modelling of the full-scale slope based on the results of numerical modelling of the scale embankment, which in turn can be verified on the basis of model tests. In this case, the data points of the diagram show the ratios of the results of the deformations of task 2 to the deformations of task 1. Thus, by multiplying the numerical simulation results of task 2 by the correction factor, we obtain the value of the task 1 deformation.

The general correction factors that allow for the adjustment of real-scale modelling displacement results of a reinforced or unreinforced embankment with the actual soil characteristics in Plaxis 2D are shown in Figure 17. In this case, the points of the diagram show the ratios of the deformation results of task 2 to the
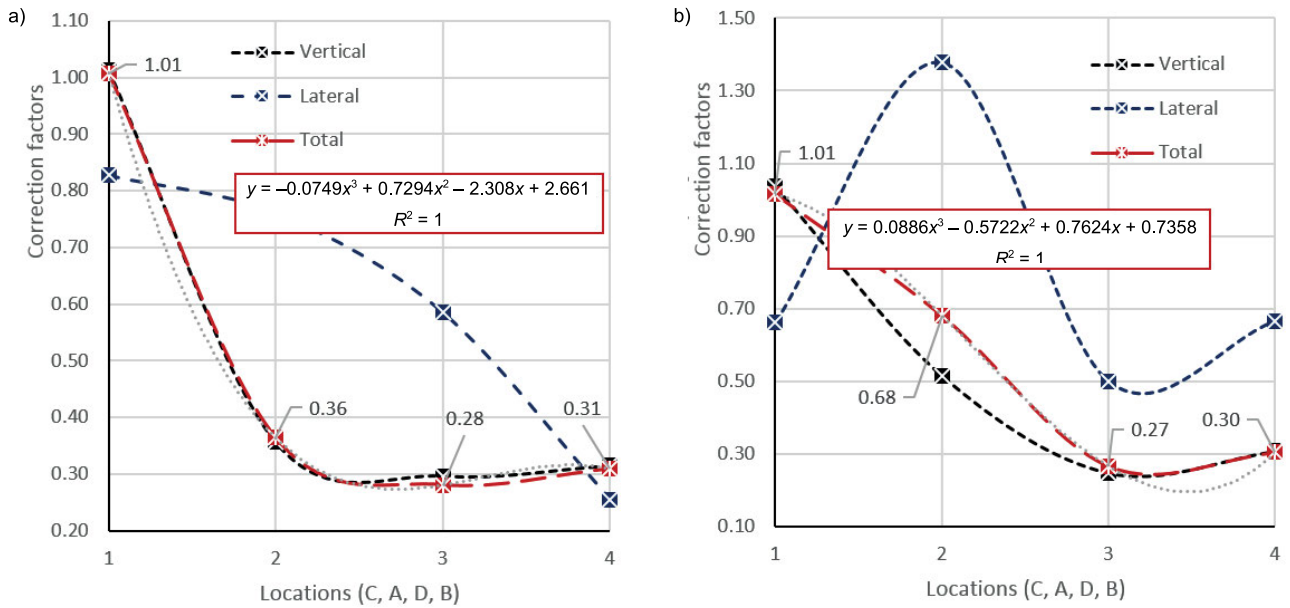
Fig. 16. Corrective actions of task 2 based on the results of task 1: a) unreinforced embankment, b) reinforced embankment; source: own study
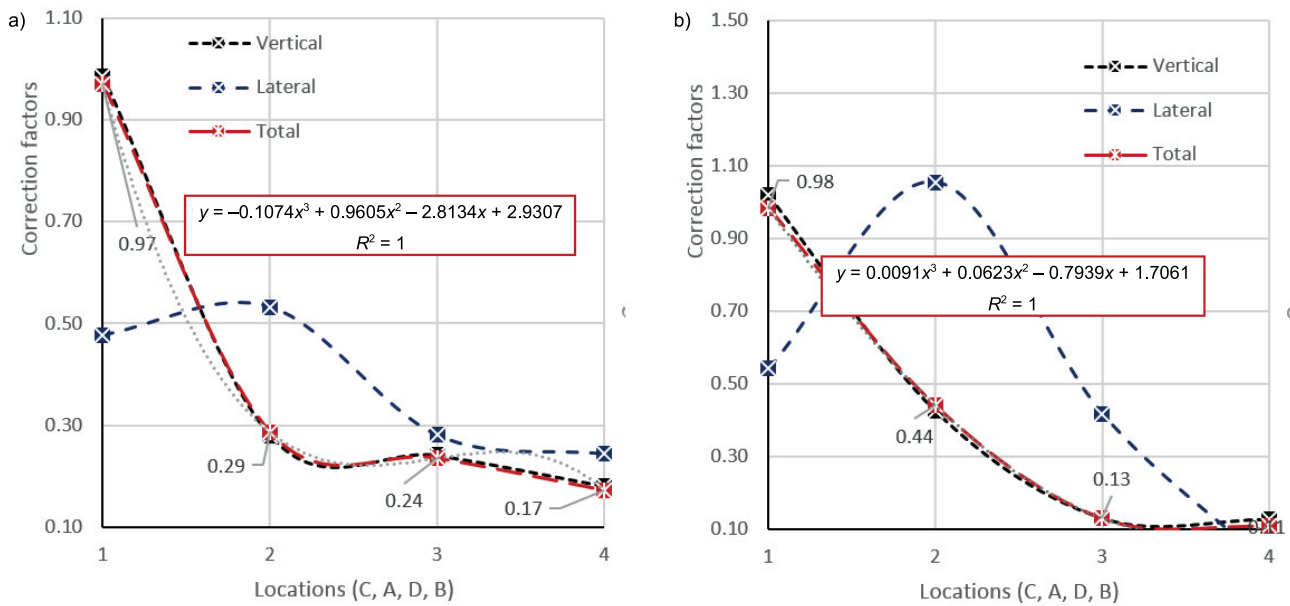

Fig. 17. Corrective actions of task 2 based on the results of task 1 and model tests: a) unreinforced embankment, b) reinforced embankment; source:

deformations of the model tests. Thus, by multiplying the numerical modelling results of task 2 by the correction factor we obtain the value of the model tests.

In general, a method for estimating the deformed state of the embankment (to assess overall stability) using numerical modelling was obtained, the results of which are corrected based on a model scale test (but still *in situ*).

CONCLUSIONS

1. To assess the effect of geosynthetic reinforcement elements on the stability of the existing soil embankment, model (scaled) tests on a scale of 1:30 and numerical modelling were performed. The test set included simulations of displacements

of the soil base underlying the embankment as a result of its washout. To assess the strain condition, the locations were selected (relative to which displacement measurements were made) at different distances from the source of a prescribed displacement.

2. The results of the embankment model tests are represented by the dependencies between the prescribed soil displacement (caused by the displacement of the sheet side walls) and the embankment deformations of the selected locations. In both cases (unreinforced and reinforced models), the maximum deformations were logically observed near the source of the specified displacement and the minimum deformations at the maximum distance from it.

According to the results of deformation comparisons between unreinforced and reinforced models, dependencies (or

equations) describing the degree of influence of reinforcement were derived. According to the analysis of the arguments of the variable equations, the maximum influence of reinforcement is observed at location B, where the variable of vertical strain is 0.0166, lateral strain is 0, and total strain is 0.0161. The minimum influence was found at locations A and C, where no reinforcement was used: the vertical deformation variable is 1 and 0.9 (respectively), the lateral is 1.04 and 1.08, and the total is 1 and 0.9.

3. The results of the numerical modelling of task 1 are also represented by the dependencies between the prescribed soil displacement and the embankment deformations of the selected locations. In general, a similar trend in the deformed behaviour of the embankment was revealed: the maximum vertical displacements in both cases (on the reinforced and unreinforced embankment) were observed at points C, the minimum ones at points B. Comparisons were made between the vertical components of the total displacement of the numerical modelling and the sheet tests. In both cases, there was a tendency for the percentage difference in the data to increase with distance from the excitation source, if near the prescribed displacement (location C) the difference averaged 3.8% and 1.3% ,unreinforced and reinforced models, respectively, then at the farthest point (location B) the difference averaged 79.5% and 180%, respectively. Based on the comparison, the correction factors (expressed as functions) of the vertical, lateral, and total displacements were obtained, depending on the distance to the source of the prescribed displacement or, in reality, on the movement of the underlying soils.

4. The results of numerical modelling of task 2 are presented by dependencies similar to task 1. The obtained deformations (vertical, lateral, and resulting) of task 2 are similar in quality of deformation to task 1, but the quantitative values are individual. Comparisons of the results of numerical simulations of task 2 to task 1 are expressed by coefficients of ratios, taken at a scale of 1:30. The analysis of obtained coefficients showed that the maximum convergence in both cases (unreinforced and reinforced models) is revealed in location C, which corresponds to the minimum ratio coefficients of 0.99 (in both cases). The minimum convergence, which corresponds to the maximum ratio coefficients is revealed in location B: 3.42 and 3.74, for unreinforced and reinforced models, respectively.

5. As a result of a set of studies, general corrective actions were obtained, allowing to reconcile the results of real-scale simulation displacements of a reinforced or unreinforced embankment with the actual ground characteristics in Plaxis 2D. Thus, in the course of the study, it was possible to obtain corrective actions that allow acceleration of the process of variation modelling, since the simulation of different design situations by the numerical method is less time-consuming compared to model tests. At the same time, the initial conditions for achieving reliable results using this estimation method remain the similarity of the engineering and geological conditions of the underlying foundation, the embankment soil, and the reinforcement elements used.

6. As a result of a set of studies, correction factors were obtained to allow for the adjustment of the results of numerical modelling of a reinforced or unreinforced embankment on a real scale with the actual ground characteristics in Plaxis 2D. Thus, in the course of the study, it was possible to obtain corrective factors

to speed up the process of variational modelling, since the simulation of different design situations by the numerical method is less time-consuming compared to model tests. In this case, the important conditions for achieving reliable results using the numerical evaluation method remain the similarity of the engineering and geological conditions of the foundational soil, the embankment, and the reinforcement elements.

CONFLICT OF INTERESTS

The author declares no conflict of interests.

REFERENCES

Abdelkrim, M. and Buhan de, P. (2007) "An elastoplastic homogenization procedure for predicting the settlement of a foundation on a soil reinforced by columns," *European Journal of Mechanics – A/Solids*, 26(4), pp. 736–757. Available at: https://doi.org/10.1016/j.euromechsol.2006.12.004.

Ahmad, H. and Mahboubi, A. (2021) "Effect of the interfacial shearing stress of soil-geogrid interaction on the bearing capacity of geogrid-reinforced sand," *Innovative Infrastructure Solutions*, 6(2), 57. Available at: https://doi.org/10.1007/s41062-020-00430-8.

ASTM D4439 (2023a) *Standard terminology of geosynthetics*. West Conshohocken: American Society for Testing and Materials.

ASTM D6637/D6637M (2023b) *Standard test method for determining tensile properties of geogrids by the single or multi-rib tensile method*. West Conshohocken: American Society for Testing and Materials.

Berg, R.R. and Collin, J.G. (1993) "Material parameters used in design of geosynthetic-reinforced soil structures," in S.C.J. Cheng (ed.) *Geosynthetic Soil Reinforcement Testing Procedures*. San Antonio, Texas, USA 19 Jan 1993. West Conshohocken: American Society for Testing and Materials. Available at: https://trid.trb.org/view/385511 (Accessed: September 25, 2024).

Chang, P.W. *et al.* (2003) "Shear strength characteristics of composite reinforced soils," in C.F. Leung *et al.* (eds.) *Proceedings of the Twelfth Asian Regional Conference on Soil Mechanics and Geotechnical Engineering*. Singapore 04–08 Aug 2003. Singapore: National University of Singapore.

Chen, M.Y. *et al.* (2013) "Numerical analysis of widened embankments with geogrid reinforcement," *Applied Mechanics and Materials*, 256–259, pp. 2004–2008. Available at: https://doi.org/10.4028/www.scientific.net/AMM.256-259.2004.

Dhanya, K.A. and Divya, P.V. (2022) "Reinforced composites for resilient reinforced soil slopes to prevent rainfall induced failures," in A. Lemnitzer and A.W. Stuedlein (eds.) *Geo-congress 2022: Soil Improvement, Geosynthetics, and Innovative Geomaterials*. Charlotte, North Carolina, USA 20–23 Mar 2022. Reston: American Society of Civil Engineers.

Ding, D.W. and Hargrove, S.K. (2006) "Nonlinear stress-strain relationship of soil reinforced with flexible geofibers," *Journal of Geotechnical and Geoenvironmental Engineering*, 132(6), pp. 791–794. Available at: https://doi.org/10.1061/(asce)1090-0241(2006)132:6(791).

El-Naggar, M.E., Kennedy, J.B. and Ibrahim, E.M. (1997) "Mechanical properties of reinforced soil," *Composites Part B-Engineering*, 28(3), pp. 275–286. Available at: https://doi.org/10.1016/s1359-8368(96)00061-3.

Hara, T. *et al.* (2010) "Independent reinforced soil structure with pile foundation – Piled geo-wall: An experimental study on the application to seismic measure for embankment," *Soils and Foundations*, 50(5), pp. 565–571. Available at: https://doi.org/10.3208/sandf.50.565.

Jiang, J.Q. (2013) "Numerical simulation of mechanical properties of reinforced red-sandstone granular soil based on 3D discrete element method," *Applied Mechanics and Materials*, 353–356, pp. 802–805. Available at: https://doi.org/10.4028/www.scientific.net/AMM.353-356.802.

Kanchi, G.M., Neeraja, V.S. and Babu, G.L.S. (2015) "Effect of anisotropy of fibers on the stress-strain response of fiber-reinforced soil," *International Journal of Geomechanics,* 15(1), 06014016. Available at: https://doi.org/10.1061/(asce)gm.1943-5622.0000392.

Kumar, S. and Roy, L.B. (2022) "Rainfall induced geotextile reinforced model slope embankment subjected to surcharge loading: A review study," *Archives of Computational Methods in Engineering.* Available at: https://doi.org/10.1007/s11831-021-09688-2.

Li, L.H. *et al.* (2018) "Shear performance of waste tires, geogrid and geocell reinforced soils," in L. Li, B. Cetin, X. Yang (eds.) *Proceedings of GeoShanghai 2018 International Conference: Ground Improvement and Geosynthetics*, pp. 463–472. Shanghai, China 27–30 May 2018. Singapore: Springer Nature. Available at: https://doi.org/10.1007/978-981-13-0122-3_51.

Lin, Y.L. (2013) "Deformation behavior of reinforced embankment slopes under seismic excitation," *Disaster Advances*, 6(7), pp. 12–19.

Lukpanov, R.E. (2016) "Laboratory modeling of soil dam reinforced by geosynthetic material," in A. Zhussupbekov (ed.) *Challenges and Innovations in Geotechnics – Proceedings of the 8th Asian Young Geotechnical Engineers Conference*, pp. 159–162. Astana, Kazakhstan 5–7 Aug 2016. London: CRC Press.

Lukpanov, R.E. and Awwad, T. (2019) "Experimental and numerical modelling of a reinforced structure," in M. Meguid, E. Guler and J.P. Giroud (eds.) *Advances in Geosynthetics Engineering. Proceedings of the 2nd GeoMEast International Congress and Exhibition on Sustainable Civil Infrastructures, Egypt 2018 – The Official International Congress of the Soil-Structure Interaction Group in Egypt (SSIGE)*, pp. 1–11. Giza, Egypt 24–28 Nov 2018. Cham: Springer. Available at: https://doi.org/10.1007/978-3-030-01944-0_1.

Sato, A. *et al.* (2014) "Frost protection for geotextile-reinforced soil walls in service," in V.M. Ulitsky *et al.* (eds.) *Advances in Soil Mechanics and Geotechnical Engineering. Proceedings of the ISSMGE Technical Committee 207 International Conference on Geotechnical Engineering. Volume 4: Soil-Structure Interaction, Underground Structures and Retaining Walls*, pp. 345–352. St Petersburg, Russia 16–19 Jun 2014. Amsterdam: IOS Press BV. Available at: https://doi.org/10.3233/978-1-61499-464-0-345.

Shin, E.C. and Young, I.O. (2006) "Case histories of geotextile tube construction project in Korea," in E.S. Shin and J.G. Kang (eds.) *Proceedings of the International Conference on New Development in Geoenvironmental and Geotechnical Engineering*. Incheon, Korea 9–11 Nov 2006. Incheon: IETeC.

Wang, L., Chen, S. and Gao, P. (2014) "Research on seismic internal forces of geogrids in reinforced soil retaining wall structures under earthquake actions," *Journal of Vibroengineering*, 16(4), pp. 2023–2034.

Zhang, M.X., Javadi, A.A. and Min, X. (2006) "Triaxial tests of sand reinforced with 3D inclusions," *Geotextiles and Geomembranes*, 24(4), pp. 201–209. Available at: https://doi.org/10.1016/j.geotexmem.2006.03.004.

Zomberg, J.G. (2007) "New horizons in reinforced soil technology," in J. Otani, Y. Miyata and T. Mukunoki (eds.) *Proceedings and Monographs in Engineering, Water and Earth Sciences. New Horizons in Earth Reinforcement. 5th International Symposium on Earth Reinforcement (IS Kyushu 07)*, pp. 25–44. Fukuoka, Japan 14–16 Nov 2007. London: CRC Press.